RSC Advances

PAPER

SPION@polydehydroalanine hybrid particles†

Moritz von der Lühe,[ab] Ulrike Günther,[ab] Andreas Weidner,[c] Christine Gräfe,[d] Joachim H. Clement,[bd] Silvio Dutz[ce] and Felix H. Schacher*[ab]

It is generally accepted that a protein corona is rapidly formed upon exposure of nanoparticles to biological fluids and that both the amount and the composition of adsorbed proteins affect the dispersion properties of the resulting particles. Hereby, the net charge and overall charge density of the pristine nanoparticles are supposed to play a crucial role. In an attempt to control both charge and charge distribution, we report on the coating of superparamagnetic iron oxide nanoparticles (SPIONs) with different polyelectrolytes. Starting from orthogonally protected polydehydroalanine, the material can be easily transformed into a polyanion (poly(*tert*-butoxycarbonyl acrylic acid), P*t*BAA), polycation (poly(aminomethylacrylate), PAMA), or even a polyzwitterion (polydehydroalanine, PDha). While coating of SPIONs with P*t*BAA and PDha was shown to be successful, approaches using PAMA have failed so far. The dispersion properties of the resulting hybrid particles have been investigated using dynamic light scattering (DLS), zeta-potential, and TEM measurements – the amount of adsorbed polymer was quantified using vibrating sample magnetometry (VSM) and thermogravimetric analysis (TGA).

Introduction

During the last decades, magnetic nanoparticles (MNP) have gained remarkable interest regarding their use in biomedical applications.[1] They are used as contrast agents for nuclear magnetic resonance imaging (MRI)[2,3] as well as in therapeutic approaches like hyperthermia,[4–7] drug targeting *via* external magnetic fields,[8–11] and targeted drug delivery. Conventional materials often cannot fulfill the strict requirements necessary for materials in biomedical applications, and therefore innovative materials are needed, where certain properties such as size, shape, charge, and charge density can be precisely controlled.

Recently, a lot of effort has been devoted to the synthesis and characterization of hybrid materials featuring inorganic magnetic cores and organic coatings. Such hybrid materials offer many options as they combine the properties of both components: the magnetic core and, thus, the opportunity of manipulation *via* external fields as well as an organic coating, which allows the adjustment of particle properties like solubility, surface charge, and particle–particle as well as particle–tissue interactions. The organic coating also enables further surface functionalization with, *e.g.*, antibodies, proteins, or dyes for medical imaging and their use in therapeutic approaches.[12] Regarding the core materials, superparamagnetic iron oxide nanoparticles (SPION) consisting of iron oxides like magnetite (Fe_3O_4) and maghemite (γ-Fe_2O_3) are of peculiar interest because of their lowered toxicity in comparison to other magnetic materials like Ni or Co at comparably high magnetizations.[13] Hereby, the inherent magnetic characteristics of the core depend on the particle size.[14] Already in 1930 it was predicted that MNPs with radii below 15 nm would consist of a single magnetic domain and feature superparamagnetic properties, *i.e.* the absence of magnetic moments in MNP without the presence of an external magnetic field.[15]

Upon the application of MNP into biological systems, a protein corona is formed due to immediate protein adsorption onto the particle surface.[16] This corona formation is influenced by a number of particle-associated factors like size, surface charge,[17,18] and incubation temperature. The temperature is supposed to influence both the formation and the composition of the protein corona,[19] whereas the particle size only seems to influence the amount of adsorbed protein but not the corona composition itself.[16] Surface charge on the other hand has an impact on the corona formation as well as the particle toxicity and cell uptake. It was already shown that positively charged nanoparticles show increased cell uptake and cytotoxicity compared to particles exhibiting negative charges.[20] However, here the focus has been put on the particle net charge whereas

aInstitute of Organic and Macromolecular Chemistry (IOMC), Friedrich Schiller University Jena, Humboldtstraße 10, 07743 Jena, Germany. E-mail: felix.schacher@uni-jena.de

bJena Center for Soft Matter (JCSM), Friedrich Schiller University Jena, Philosophenweg 7, 07743 Jena, Germany

cInstitute of Biomedical Engineering and Informatics, Technische Universität Ilmenau, 98693 Ilmenau, Germany

dKlinik für Innere Medizin II, Abteilung Hämatologie und Internistische Onkologie, Universitätsklinikum Jena, 07743 Jena, Germany

eDepartment of Nano Biophotonics, Leibniz Institute of Photonic Technology, 07745 Jena, Germany

† Electronic supplementary information (ESI) available. See DOI: 10.1039/c5ra01737h

the influence of charge density so far has not been investigated. An elegant way to adjust the surface charge of magnetic nanoparticles is *via* different coating materials. In that respect, different polyelectrolyte coatings for inorganic nanoparticles are described in the literature, often adsorbed to the particle surface using layer by layer (LBL) techniques based on attractive electrostatic forces.[21] In 2004, the preparation of magnetite MNPs coated with poly(allylamine hydrochloride) (PAH) by LBL approaches was reported where PAH was adsorbed onto negatively charged MNPs at pH = 8.[22]

Also, LBL multishell hybrid particles labeled with poly(9,9-di [3′-(1-ethyl-1,1-dimethylammonio)propyl]2,7-fluorenyl-*alt*-1,4-phenylene dibromide),[23] coated with poly(acrylic acid) (PAA),[24] or natural polyelectrolytes like alginate[25] and chitosan for drug delivery applications[11] have been described. Wotschadlo *et al.* reported the encapsulation of SPION aggregates within alternating layers of carboxymethyldextran (CMD) and poly-(diallyldimethylammonium chloride) (PDADMAC).[26] They also investigated the influence of shell composition on subsequent interactions of these hybrid materials with cells, with the result that CMD shows rapid uptake into tumor cells, whereas carboxymethylated cellulose and pullulan show interactions with tumor cells as well as with leukocytes.[27] Another example, rather focusing on heterogeneous catalysis, used amino cellulose as coating for SPIONs. The resulting Fe_3O_4@amino cellulose MNPs could then be used as heterogeneous catalysts in atom transfer radical polymerizations of styrene.[28] Also, "*grafting from*" strategies starting from SPIONs have been analyzed quantitatively.[29]

Our work focuses on the preparation of hybrid nanoparticles featuring a SPION core, consisting of both maghemite (γ-Fe_2O_3) and magnetite (Fe_3O_4), and a polyelectrolyte shell. The polymer we employ as organic coating can be selectively transformed into a polycation, polyanion, or even a polyzwitterion without variations of the polymer backbone being necessary. Starting from poly(*tert*-butoxycarbonylamino methylacrylate) (P*t*BAMA), a

material which carries both a protected amino group (*tert*-butoxycarbonyl, *boc*) and a protected carboxylic acid group (methyl ester), each group can be deprotected separately. This leads to either polycationic poly(aminomethyl acrylate) (PAMA), polyanionic poly(*tert*-butoxycarbonylamino acrylic acid) (P*t*BAA), or in the case of complete deprotection, to polyzwitterionic poly(dehydroalanine) (PDha, Scheme 1).[30]

Magnetite MNP with 8 nm in diameter have been successfully coated with both P*t*BAA and PDha in different amounts. The obtained hybrid particles have been characterized by dynamic light scattering (DLS), zeta-potential measurements, vibrating sample magnetometry (VSM), and transmission electron microscopy (TEM). Whereas P*t*BAA and PDha readily seem to form adsorbed layers on MNP, up to now this could not be achieved in case of PAMA due to solubility issues. First *in vitro* biocompatibility assays revealed no cytotoxic effects of both P*t*BAA and PDha.

Results and discussion

Synthesis of polyelectrolytes

Poly(*tert*-butoxycarbonylamino methacrylate) (P*t*BAMA) was synthesized *via* free radical polymerization (FRP) using Lucirin-TPO® as UV-photoinitiator. Compared to our earlier study,[30] we also used solution polymerization in 1,4-dioxane (50 wt%) as, in this case, it was possible to obtain materials with molar masses below 50 000 g mol^{-1} in a straightforward manner. The reason for using P*t*BAMA with molar masses below 50 000 g mol^{-1} is that we anticipated the encapsulation of single MNPs to be achieved more easily compared to longer polymer chains. After 5 minutes under UV exposure, the polymerization was stopped and materials with a molar mass of $M_w = 43\,000$ g mol^{-1} according to size exclusion chromatography (DMAc as solvent, poly(methyl methacrylate) (PMMA) calibration) could be obtained. The purification was carried out by dialysis against methanol.
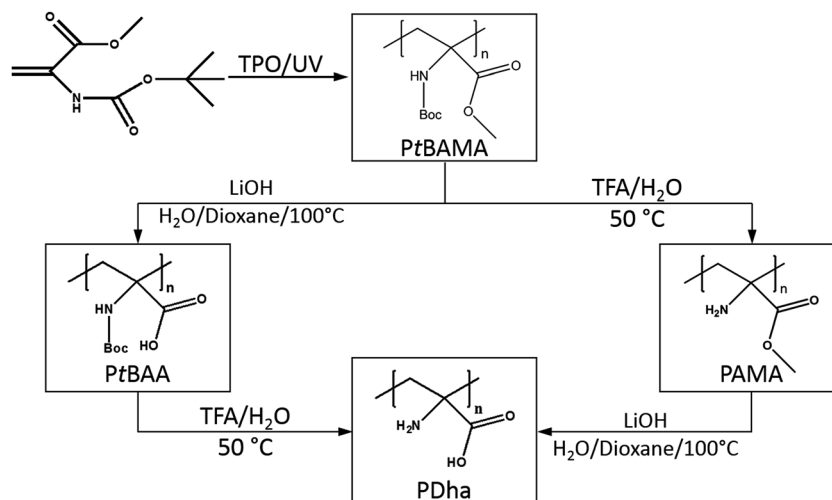
Scheme 1 Synthesis and polymerization of *t*BAMA, followed by deprotection leading to poly(*tert*-butoxycarbonylamino acrylic acid) (P*t*BAA), poly(aminomethyl acrylate) (PAMA), and poly(dehydroalanine) (PDha).

Table 1 Polymerization conditions and analytical data of P*t*BAMA

Sample	M : I (n : n)	M_n^a [kg mol^{-1}]	M_w^a [kg mol^{-1}]	$Đ^a$	M_w^b [kg mol^{-1}]	Yield
P*t*BAMA$_{184}^c$	200 : 1	23	43	1.89	37	52%

^{a} Determined by DMAc SEC, PMMA calibration. ^{b} Determined by SLS in MeOH. ^{c} Obtained by solution polymerization in 1,4-dioxane (50 wt%); all DPs were calculated from M_w determined by SLS.

The obtained polymer was characterized using NMR spectroscopy (Fig. S1†) as well as SEC measurements (Fig. S2†). The ^{1}H-NMR-spectrum of P*t*BAMA was measured in CDCl$_3$ and shows signals at $\delta = 5.4$ ppm (b, 1H) for the amino function, $\delta = 3.7$ ppm (3H) for the methyl ester and $\delta = 1.4$ ppm (11H) for the boc protective group and the polymer backbone according to literature.[30] SEC measurements in DMAc (Fig. S2†) revealed the molar masses shown in Table 1. As SEC only provides apparent values, we also used static light scattering (SLS) in MeOH with concentrations ranging from 0.5 to 5 g L^{-1} (Fig. S3†). In contrast to earlier studies, SLS yielded slightly lower M_w values (37 000 g mol^{-1}, leading to P*t*BAMA$_{184}$ with the subscripts denoting the degrees of polymerization) than obtained by SEC. At this point, we explain this by certain polymer–column interactions, which also might explain the tailing observed in the SEC elugrams.

Next, P*t*BAMA was partially deprotected to either poly-(aminomethyl acrylate) (PAMA) or poly(*tert*-butoxycarbonylamino acrylic acid) (P*t*BAA). For alkaline deprotection of the methyl ester, P*t*BAMA was stirred with 14 equivalents of LiOH in a 1,4-dioxane–water mixture (1/1) at 100 °C for 3 hours. The product (P*t*BAA$_{184}$) was purified by dialysis against water. ^{1}H-NMR in D$_2$O/NaOD with pD = 12 showed signals at $\delta = 2.7$ ppm (b, 2H for the polymer backbone) and $\delta = 1.3$ ppm (s, 9H) for the boc-protective group.

PAMA was obtained by acidic deprotection of the boc protective group in P*t*BAMA. Therefore, P*t*BAMA was stirred in trifluoro acetic acid at 50 °C for 1 hour and the product was purified by subsequent precipitation in methanol. The ^{1}H-NMR spectrum measured in DMSO-d$_6$ shows signals at $\delta = 3.6$ ppm (3H) for the methyl ester and $\delta = 2.1$ ppm (2H) for the polymer backbone. Also, ^{13}C-NMR measurements show the absence of the signal at $\delta = 153$ ppm for the boc protective group. PAMA was then further treated with LiOH at 100 °C for 3 hours to obtain completely deprotected polydehydroalanine (PDha).

The obtained polyelectrolytes exhibit very different solubilities. Both, the polyanionic P*t*BAA and the polycationic PAMA only dissolve at pH values higher than 10, in case of PAMA unfortunately under partial deprotection of the boc protective group. The fully deprotected PDha is directly soluble in alkaline media of pH = 8 or higher, but can be brought to lower pH values by subsequent titration steps. For biocompatibility tests, the polyelectrolytes were dissolved at pH = 8 (PDha$_{184}$) and pH = 10 (P*t*BAA$_{184}$) with 5 g L^{-1} and then titrated to pH = 7 using small aliquots of 1 M HCl.

Biocompatibility of PDha and P*t*BAA

In order to validate the biocompatibility of both polyanionic and polyzwitterionic polyelectrolytes (PAMA was not tested – again due to solubility issues), *in vitro* viability studies were performed. Human brain microvascular endothelial cells (HBMEC) serving as sensitive cell culture model representing the human blood–brain barrier were exposed to increasing concentrations of P*t*BAA$_{184}$ or PDha$_{184}$ for indicated durations and subsequently subjected to a fluorescence-based viability assay. As can be seen, both PDha$_{184}$ and P*t*BAA$_{184}$ do not exert cytotoxic effects on HBMEC up to a concentration of 75.6 μg mL^{-1} and over a 24-hour treatment period (Fig. 1).

Synthesis of the SPION core

The nanoparticles were synthesized by co-precipitation of FeCl$_2$ and FeCl$_3$ in alkaline media as described earlier.[31] The pristine particles are stabilized in acidic media (pH = 2) due to repulsive electrostatic forces resulting from positive surface charges. Table 2 shows number-weighted particle size distributions, obtained from CONTIN analysis of the measured autocorrelation functions at different pH values.
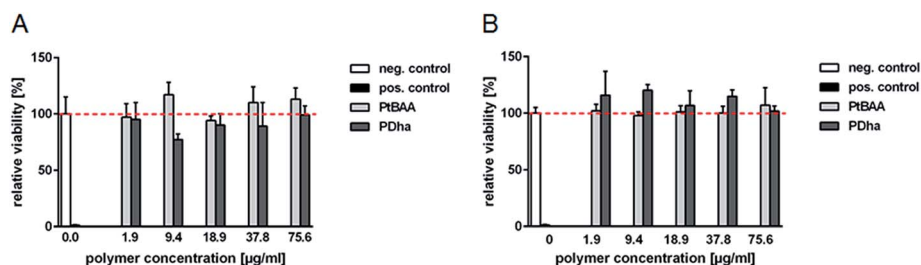

Fig. 1 Increasing concentrations of PDha$_{184}$ and P*t*BAA$_{184}$ do not affect viability of HBMEC; HBMEC cultures were incubated with both polymers for 3 h (A) or 24 h (B) with concentrations as indicated. neg. control: MilliQ water, negative control with regard to cytotoxicity; pos. control: detergent TritonX100 (final conc. 0.02% (v/v)), positive control with regard to cytotoxicity.

Table 2 Hydrodynamic diameters of SPIONs at different pH values determined *via* DLS

| pH	d_{DLS} after ultrasonication [nm]
2	8
6	8
12	22

They show an average diameter of 8 nm at pH = 2 which was also confirmed by transmission electron microscopy (TEM: d = 12 ± 2 nm, Fig. S3 and S4†). The DLS CONTIN-plot at pH 7 is also included in Fig. 3A–C. At pH-values >7 aggregation of the SPION cores occurred, followed by precipitation after several minutes. Characterization with vibrating sample magnetometry (VSM) showed prevailing superparamagnetic properties, *i.e.* a high saturation magnetization Ms ($72 \text{ Am}^2 \text{ kg}^{-1}$) and low coercivity Hc (1.6 kA m^{-1}). The particle diameter of 8.3 nm from VSM (Chantrell method) is in good agreement with DLS at pH values up to 6. The hysteresis loop is shown together with those of the hybrid particles after coating with P*t*BAA or PDha in Fig. 5.

TGA measurements of the pristine particles under inert atmosphere show a weight loss of 3.3% in three steps. The first step from 20 to 125 °C (1.1%) can be attributed to the evaporation of adsorbed water. The second step from 200 to 500 °C (1.4%) might result from a phase transformation of a small amount of impurity phases (hydrated oxides and hydroxides of iron) to hematite, and during the last step from 500 to 800 °C (0.8%) remaining salts and carbonates trapped inside the particles evaporate. The corresponding thermogram is depicted together with those for the hybrid particles after coating with P*t*BAA or PDha in Fig. 4.

Nanoparticle coating

As discussed above, SPIONs form stable dispersions in acidic media whereas both P*t*BAA and PDha are soluble at pH values above 7. In case of PAMA, DMSO as organic co-solvent had to be employed to ensure solubility. Therefore, separate coating conditions had to be found for each combination of polyelectrolyte and SPION (Scheme 2).

P*t*BAA/PDha. The SPIONs were washed, dispersed in MilliQ water/HCl at pH = 2 (1 g L^{-1}) and added to solutions of P*t*BAA$_{184}$ or PDha$_{184}$ in MilliQ/NaOH at pH = 12 (each 2 g L^{-1}). After ultrasonication for 1 h at 50 °C, the mixture was centrifuged at 8000 rpm, the supernatant was removed and the resulting SPION@polyelectrolyte hybrid particles were washed with deionized water. Afterwards, the solubility was investigated. ζ-potential measurements for both, SPION@P*t*BAA and SPION@PDha showed distinct changes in comparison to the pristine particles (+31.7 mV at pH = 7, Fig. 2A and B). Depending on the amount of used polyelectrolyte, SPION@P*t*BAA$_{184}$ hybrid particles show ζ-potentials of +5.3 mV (m : M, MNP : polymer 1 : 2) down to −31.8 mV (1 : 8) at pH = 7 (Fig. 2A). The values for SPION@PDha$_{184}$ at pH = 7 also decrease to values between +11.2 (1 : 8) and +14.9 (1 : 2).
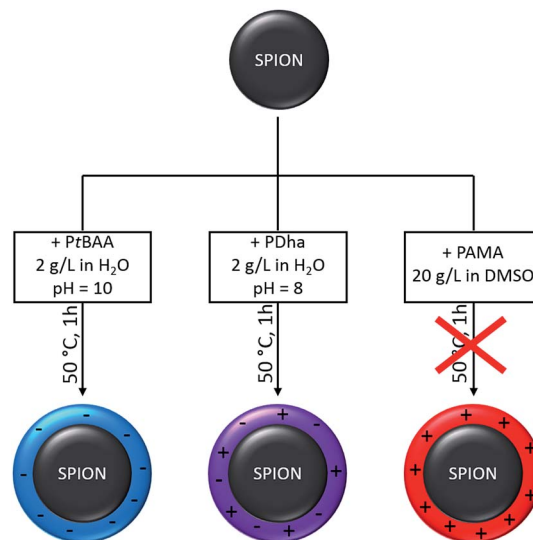
Scheme 2 SPION coating with different polyelectrolytes – P*t*BAA (left), PDha (middle), and PAMA (right), leading to SPION@polyelectrolyte hybrid particles with different surface charge.

The changes in surface charge directly influence the dispersion stability of SPION@P*t*BAA$_{184}$ and SPION@PDha$_{184}$. Whilst pristine SPIONs showed good dispersion stability under acidic conditions up to pH = 7, both SPION@P*t*BAA$_{184}$ and SPION@PDha$_{184}$ behaved differently: stable dispersions were formed at higher pH values (Fig. 2C), whereas precipitation occurred upon pH = 7 or lower in case of SPION@P*t*BAA$_{184}$. SPION@PDha$_{184}$ forms stable dispersions under acidic conditions and shows precipitation at pH = 7 if not agitated, but can be redispersed using, *e.g.* ultrasound. We attribute this to successful adsorption of material on the particle surface and the fact that SPION@PDha$_{184}$ is only partially stable at pH = 7 can be attributed to the isoelectric point of PDha which has been determined to be around pH 6.6 in earlier studies.[30]

PAMA. For the attempted coating with PAMA$_{184}$, a dispersion of SPIONs at pH = 4 (1 g L^{-1}) was added to a solution of PAMA$_{184}$ in DMSO (20 g L^{-1}). The particles treated in that way show no difference in dispersion stability in comparison to particles that were dispersed and washed with DMSO without PAMA. DLS measurements show a small change in particle size of about 2 nm. The zeta potential of the particles did also not change significantly in comparison to the pristine particles after treatment with DMSO (+24.3 mV in comparison to +25.7 mV for pristine particles after treatment with DMSO). Up to now, coating of SPIONs with PAMA$_{184}$ seems not to work (see also Discussion later).

Due to certain agglomeration of the hybrid particles occurring independent of the polymer used for surface modification, DLS results regarding changes in particle size are difficult to interpret quantitatively. We therefore relied mostly on TEM measurements to determine the average sizes of SPION@polyelectrolyte hybrid particles. In all cases, TEM data showed only a slight increase in particle diameter (Fig. 3, see also Table 3). For the size determination, 100 particles from
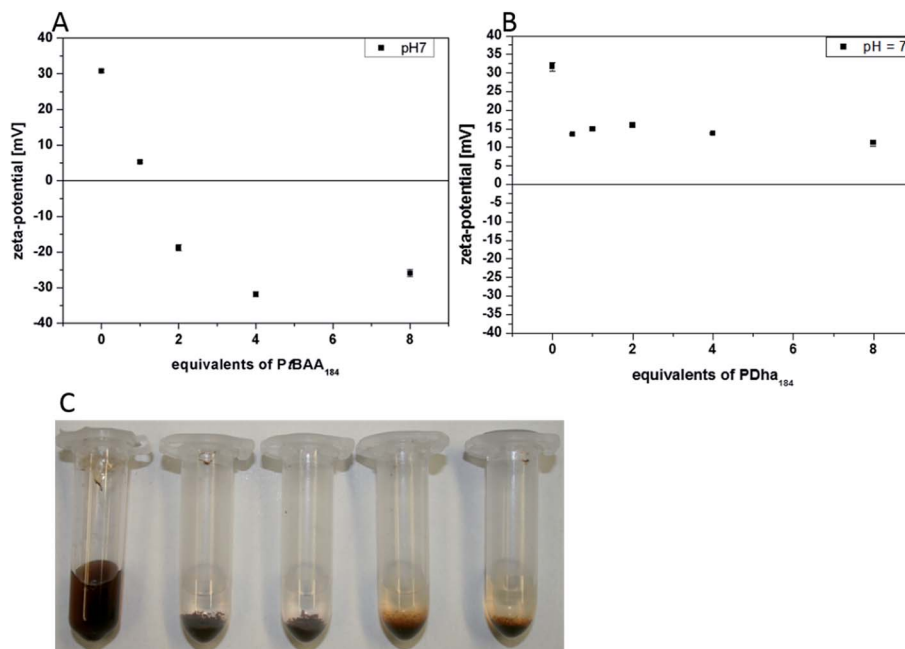
Fig. 2 ζ-potentials of SPION@PtBAA$_{184}$ at pH = 7 at different Fe : polymer ratios (A) and SPION@PDha$_{184}$ (B) at pH = 7; (C) dispersion properties of pristine MNP (left) and SPION@PDha$_{184}$ at different Fe : polymer ratios (1 : 1, 1 : 2, 1 : 4 and 1 : 8; C) at pH = 7.

different micrographs of the same sample were measured to estimate the mean diameter.

The number weighted DLS measurements show strongly increased particle diameters after the addition of PtBAA$_{184}$. The pristine particles show a diameter of 8 nm, which is increased to 354 nm after the addition of 1 equivalent of PtBAA$_{184}$ (Fig. 3A). This hints towards strong agglomeration of the coated particles. The formed agglomerates show decreasing apparent sizes with increasing polyelectrolyte content: 226 nm for 2, 103 nm for 4 and 40 nm for 8 equivalents. This can be interpreted as an increase in particle stability. The particle size determined from TEM micrographs shows almost no changes as the polyelectrolyte shell cannot be observed due to large differences in the electron density between core and shell material. The particle sizes were determined to 13 ± 3 nm after the addition of 1 eq. PtBAA$_{184}$, 12 ± 3 nm (2 eq.), 13 ± 2 nm (4 eq.), and 12 ± 3 nm (8 eq.). The size distributions are included in the ESI (Fig. S5†). Nevertheless, TEM micrographs show decreasing agglomerate sizes with increasing polyelectrolyte content as well (Fig. 3D and G). In case of SPION@PDha$_{184}$, the DLS measurements exhibit no trend for particles coated with different amounts of PDha. After the addition of 0.5 mass equivalents PDha$_{184}$, the DLS measurement shows a particle size of 13 nm. After 1 equivalent PDha added, the size is determined to 3 nm, 32 nm after 2 equivalents, 23 nm after 4 equivalents and 5 nm after 8 equivalents (Fig. 3B). TEM data revealed comparable particle diameters of 13 ± 3 nm after the addition of 0.5 and 1 eq. PDha$_{184}$, 12 ± 2 nm (2 eq.), 14 ± 3 nm (4 eq.), and 13 ± 3 nm (8 eq.). The size distributions are shown in Fig. S6.† For the TEM micrographs of the particles coated with 8 equivalents PDha$_{184}$, the grey shade around the SPION cores might indicate the presence of a polymer shell of 2–5 nm

(Fig. 3H, indicated by red arrows). Fig. 3C shows the number weighted size distribution functions as obtained from CONTIN analysis of the measured time autocorrelation functions of SPION@PAMA. As the measurements were carried out in DMSO, the sizes are not directly comparable with the other measurements. The particle size is shifted to slightly smaller values, but the particle size determined from TEM micrographs did not change significantly in comparison to the pristine particles.

The changes in dispersion stability and the results from TEM after treatment of SPIONs with solutions of PtBAA$_{184}$ and PDha$_{184}$ indicate a successful coating. To further quantify the amount of adsorbed polymer, both thermogravimetric analysis (TGA) and vibrating sample magnetometry (VSM) measurements were performed. The TGA measurements were realized under argon in a temperature range from 20–800 °C and at a heating rate of 10 K min^{-1}. Both SPION@PtBAA$_{184}$ and SPION@PDha$_{184}$ hybrid particles show increasing weight loss with increasing amounts of polymer adsorbed to the particle surface (Fig. 4).

For SPION@PtBAA$_{184}$, TGA data show only one main decomposition step between 200 and 800 °C. The remaining masses are 97% for a 1 : 1 ratio (Fe : polymer), 91% (1 : 2), 87% (1 : 4) and 88% in case of a 1 : 8 ratio (Fig. 4A). Comparable values for the addition of 4 and 8 equivalents hint towards saturation of the particle surface during shell formation. The weight loss during heating of SPION@PDha materials also occurs in three steps, similar to the observation made earlier for the pristine particles. The first step occurs up to 160 °C and can be attributed to the release of water embedded within the polymer shell. The next step between 200 and 500 °C is distinctly increased in comparison to the pristine particles, and
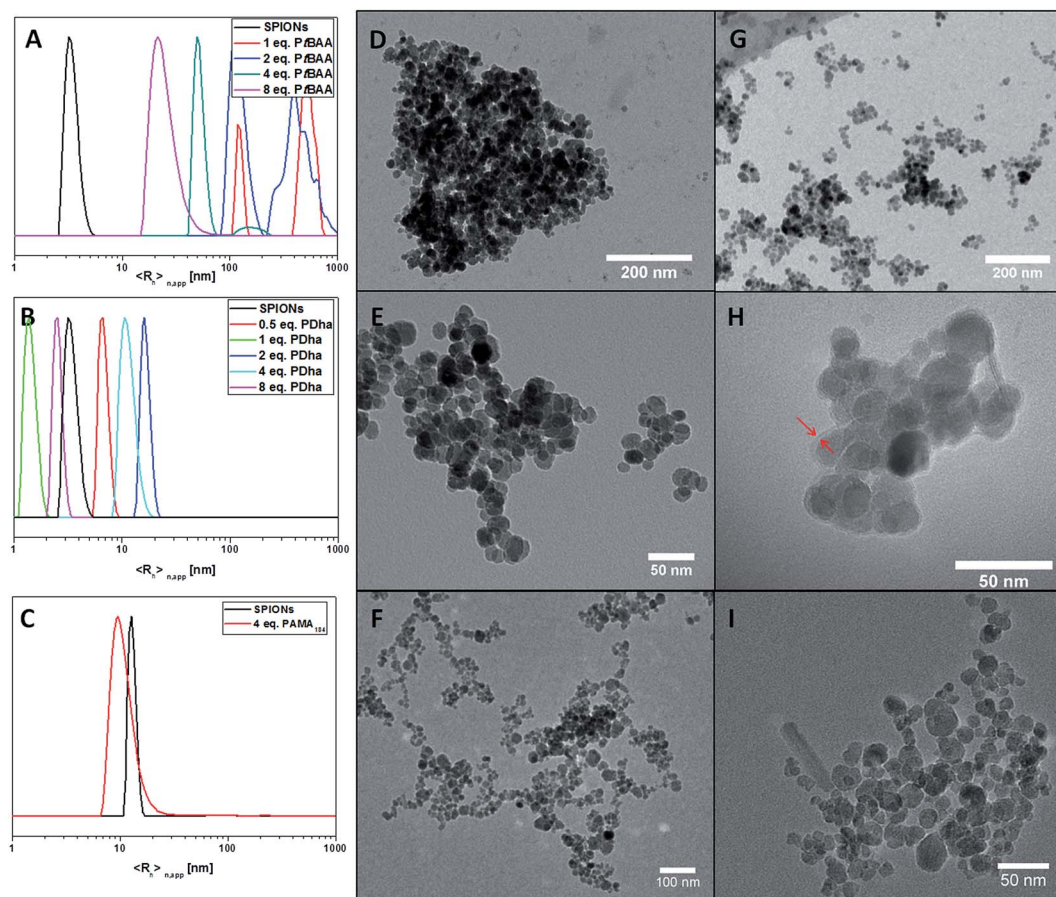
Fig. 3 Particle sizes of (A) SPION@PtBAA$_{184}$, (B) SPION@PDha$_{184}$, and (C) SPION@PAMA$_{184}$ as determined by DLS; TEM micrographs of SPION@PtBAA$_{184}$ with 1 (D) and 8 equivalents (G) PtBAA$_{184}$; SPION@PDha$_{184}$ with 1 (E) and 8 equivalents (H) PDha$_{184}$; and (F) SPION@PAMA$_{184}$ (higher magnification shown in (I)).

the last step between 500 and 800 °C again is comparable but slightly shifted to higher temperatures. This might be explained by remaining degradation products on the particle surface that hinder the evaporation of carbonate salts. In case of the particles coated with 8 equivalents of PDha$_{184}$, both the last two steps are strongly increased and are not separated as observed for the other cases. The overall weight loss is 4.3% for 0.5

equivalents PDha$_{184}$, 4% for 1, 4.6% for 2, 3.9% for 4 and 7.7% for 8 equivalents of PDha$_{184}$ (Fig. 4B). Deducting the 3.3% weight loss of the pristine particles, this leads to polymer contents of 1% for 0.5, 0.6% for 1, 1.3% for 2, 0.6% for 4, and 4.4% for 8 equivalents of PDha. The TGA measurement of SPION@PAMA$_{184}$ shows only 5% weight loss, which would represent an adsorption of 1.7% – nevertheless, the unaltered

Table 3 Summary of analytic data of SPIONs and particles coated with different polyelectrolytes

| Sample	Eq. PE	d_{DLS} [nm]	d_{TEM} [nm]	Weight loss TGA [%]	ζ-potential (pH = 7) [mV]	r_s calc. from eqn (1) [nm]	Ms [Am² kg⁻¹]
SPIONs		8	12 ± 2	3.3	31.7	—	72
SPION@PtBAA$_{184}$	1	354	13 ± 3	3	5.3	1.5 ± 0.5	65.4
SPION@PtBAA$_{184}$	2	226	12 ± 3	9	−18.8	4.2 ± 1.4	64.3
SPION@PtBAA$_{184}$	4	103	13 ± 2	13	−31.8	6.8 ± 1.7	61.5
SPION@PtBAA$_{184}$	8	40	12 ± 3	12	−25.9	6.5 ± 1.6	60.8
SPION@PDha$_{184}$	0.5	14	13 ± 3	1.0	13.5	2.2 ± 0.7	65.6
SPION@PDha$_{184}$	1	3	13 ± 3	0.6	14.9	1.8 ± 0.6	71.2
SPION@PDha$_{184}$	2	32	12 ± 2	1.3	16.0	2.4 ± 0.8	68.5
SPION@PDha$_{184}$	4	23	14 ± 3	0.6	13.8	1.8 ± 0.6	68.5
SPION@PDha$_{184}$	8	5	13 ± 3	4.4	11.2	3.6 ± 1.2	65.9
SPION@PAMA$_{184}$	4	10	12 ± 3	1.7	24.3	—	—
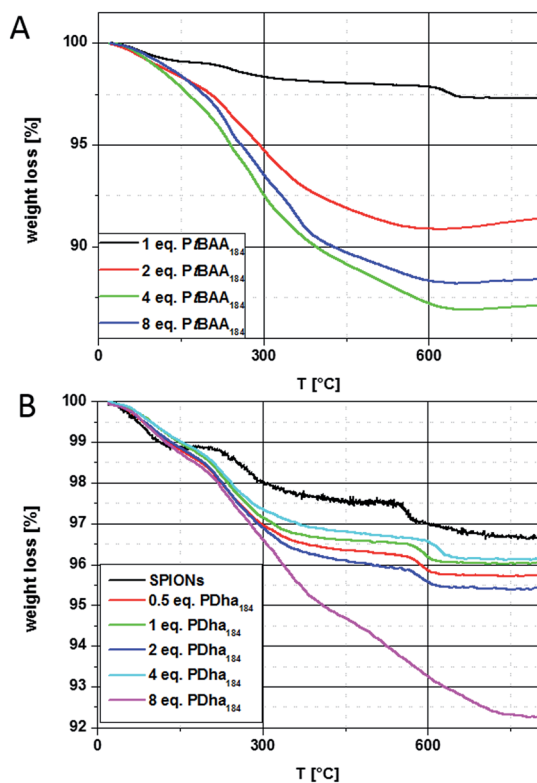
Fig. 4 Thermogravimetric analysis of (A) SPION@PtBAA$_{184}$ with 1 (black solid line), 2 (red line), 4 (green line) and 8 (blue line) equivalents of PtBAA$_{184}$ added showing distinct increasing weight loss, and (B) SPION (black line), SPION@PDha$_{184}$ with 0.5 (red line), 1 (green line), 2 (blue line), 4 (cyan line), and 8 equivalents PDha$_{184}$ (pink line) added, approximately 7.7% weight loss in total.

dispersion properties in this case rather hint towards the adsorption of DMSO on the particle surface.

Using eqn (1), the polymer shell thickness r_s can be calculated, using the radius of the core r_c as determined by DLS and TEM, the density of Fe$_3$O$_4$ ρ_c (approximately 5.2 g cm^{-3}), the density of the shell ρ_s, the weight loss wl and the residual mass

rm, both determined by TGA. The density of the polymers has been determined using a 5 mL pyknometer and hexane as liquid phase.

$$\rho(\text{P}t\text{BAA}_{184}) = 0.918 \text{ g mL}^{-1}; \ \rho(\text{PDha}_{184}) = 1.11 \text{ g mL}^{-1}$$

$$r_{\text{s}} = \sqrt[3]{r_c{}^3 \frac{\rho_{\text{c}}}{\rho_{\text{s}}} \frac{\text{wl}}{\text{rm}}} \qquad (1)$$

The calculated values are depicted in Table 3. The resulting shell thicknesses for SPION@PtBAA$_{184}$ are: 1.5 nm for 1 equivalent, 4.2 nm for 2 equivalents, 6.8 nm for 4 equivalents, and 6.5 nm for 8 equivalents. For SPION@PDha$_{184}$ the calculations reveal shell thicknesses of 2.2 nm for 0.5 equivalents, 1.8 nm for 1 equivalent, 2.4 nm for 2 equivalents, 1.8 nm for 4 equivalents and 3.6 nm for 8 equivalents. Please note that these calculations use several approximations and, hence, these values are best treated as rough estimations. Nevertheless, coatings with a thickness in the range of 1–6 nm confirm results from DLS and TEM and, to our opinion, are realistic, taking into account that also loosely adsorbed material can contribute to these values in TGA. As mentioned before, the shell thicknesses determined from TEM micrographs for SPION@PDha$_{184}$ with 8 equivalents of PDha$_{184}$ vary from 2–8 nm, which is in the range of the calculations presented above.

VSM measurements were additionally performed to investigate the magnetic properties of the particles before and after coating with a polyelectrolyte shell. For VSM measurements, the sample is placed in a uniform magnetic field and the sample holder vibrates along the z-axis. The magnetic moment of the sample induces a voltage in the four pickup-coils, which is proportional to the magnetic moment. This allows measurements of the magnetization in dependence on the magnetic field and provides the saturation magnetization (Ms) and the coercivity (Hc) of magnetic nanoparticles. According to VSM measurements, both for SPION@PtBAA$_{184}$ and SPION@PDha$_{184}$ superparamagnetic
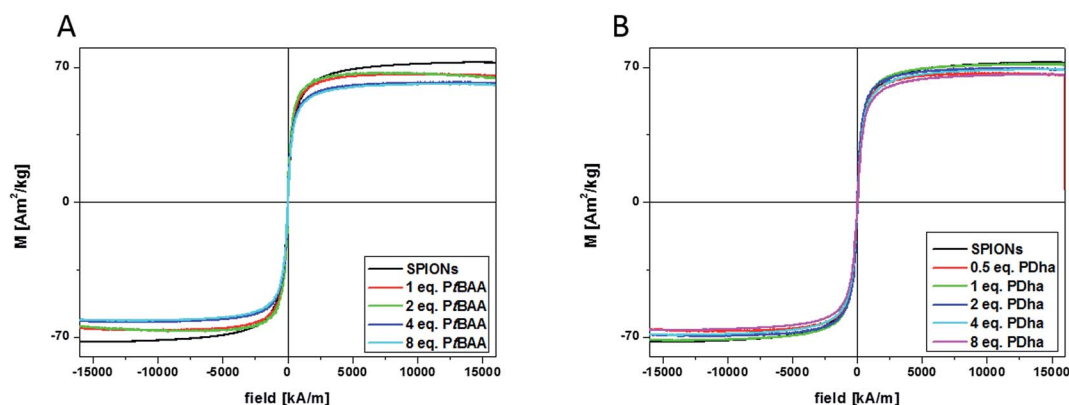

Fig. 5 VSM measurements of different polymer coated SPION NP: (A) pristine SPIONs (black line) and coated with 1 (red line), 2 (green line), 4 (blue line), and 8 (cyan line) equivalents of PtBAA$_{184}$, showing distinct decreasing Ms; (B) pristine MNP (black line) and coated with 0.5 (red line), 1 (green line), 2 (blue line), 4 (cyan line), and 8 (pink line) equivalents of PDha$_{184}$.

behavior is retained, but distinctly lowered saturation magnetizations due to adsorbed non-magnetic material (Fig. 5) can be observed. According to this data, for a Fe : polymer ratio (PtBAA$_{184}$) of 1 : 1 9.2 wt% of nonmagnetic material are adsorbed, 10.7% for ratio 1 : 2, 14.6% in case of 1 : 4, and 15.6 wt% in case of 1 : 8. Except for the ratio 1 : 1, these values are in good agreement with the values obtained by TGA measurements. For the addition of PDha$_{184}$, a decrease of 8.8% can be seen already for a 2 : 1 ratio. In case of 1 : 1, Ms is only decreased by 1.2%, 4.8% decrease are shown for 2 and 4 equivalents of PDha$_{184}$ and 8.5% for 8 equivalents. Except for the 2 : 1 ratio, the amounts of adsorbed non-magnetic material according to VSM measurements show the same trend as the TGA measurements, although the values obtained are slightly higher.

In case of SPION@PAMA$_{184}$, no changes in saturation magnetization (Ms) were found, confirming our assumptions drawn earlier during discussion of the dispersion properties. We speculate that PAMA is not adsorbed on the particle due to the protected carboxylic acid and the lower affinity of iron to nitrogen. It is also possible that the SPION surface is influenced by the presence of large amounts of DMSO. In further studies, as an alternative a catechol-functionalized PAMA derivative will be used – although this will then represent an entirely different grafting strategy.

Conclusion

We have investigated the adsorption of partially or fully deprotected polydehydroalanines onto the surface of SPIONs. Three different polyelectrolytes based on the protected polydehydroalanine were synthesized by polymerization and consecutive deprotection of either one or both of the protected functionalities. According to TGA, VSM and zeta-potential measurements, coating of SPIONs with the two materials featuring a carboxylic acid functionality (PtBAA and PDha) in different amounts was successful, whereas coating with the polycationic PAMA could not be achieved so far. We attribute this to the repulsion due to the positive surface charges of both, the pristine particles and PAMA, as well as to solubility issues.

Further work will focus on the PAMA adsorption as well as on charge control by adjusting the adsorbed amount of polyelectrolyte. The formed hybrid SPION@polyelectrolyte nanoparticles will furthermore be used for the investigation of the influence of charge and charge density on the corona formation by incubation of the particles in biological fluids.

Experimental part

Chemicals were purchased from Sigma-Aldrich or Carbolution (Saarbrücken, Germany) in p.a. grade and used without further purification. The photoinitiator Lucirin-TPO was kindly provided by BASF.

Synthesis of poly(*tert*-butoxycarbonylaminomethyl acrylate) (PtBAMA)

Free radical polymerization in the bulk: to a solution of 500 mg (2.485 mmol) tBAMA in 2.5 mL acetone 17 mg (0.0497 mmol) TPO (M : I = 50 : 1) were added. The solution was degassed with argon until acetone was completely removed. During these steps, the reaction vial was protected with aluminum foil. Then the solution was placed in a UV-cube (250 W) for 2 hours.

The clear solid was redissolved in methanol and precipitated in a mixture of ethyl acetate and hexane (1 : 4). Yield: 90%.

Free radical polymerization in solution: a solution of 2.9 mg (0.0084 mmol) TPO in 300 μL 1,4-dioxane was added to 300 mg (1.49 mmol) of tBAMA (M : I = 200 : 1). The mixture was placed in an UV-cube (250 W) for 5 minutes. The polymer was precipitated in a mixture of ethyl acetate and hexane (1 : 4). Yield: 52%.

^{1}H-NMR. (300 MHz, $CDCl_3$): δ = 5.4 (b, 1H, NH), 3.7 (3H, OCH$_3$), 1.4 (9H, Boc).

^{13}C-NMR. (300 MHz, $CDCl_3$): δ = 172.2 (COOMe), 153.9 (COOC(CH$_3$)$_3$), 79.9 (COOC(CH$_3$)$_3$), 60.2 (backbone), 52.9 (COOMe), 30.9 (backbone), 28.6 (COOC(CH$_3$)$_3$).

Synthesis of poly(*tert*-butoxycarbonyl aminoacrylic acid) (PtBAA)

6 mg TPO were added to a solution of 300 mg tBAMA in 300 μL 1,4-dioxane (50 wt%, M : I = 100 : 1). The mixture was placed in a UV cube for 5 minutes. Another 300 μL dioxane and a solution of 1.5 g LiOH in 6 mL H$_2$O were added. The mixture was stirred at 100 °C for 3 hours and neutralized with diluted HCl$_{aq.}$. During the neutralization, PtBAA precipitated. Yield: 38%.

^{1}H-NMR. (300 MHz, $D_2O/NaOD$): δ = 2.7 (b, 2H, CH$_2$), 1.3 (s, 9H, Boc).

Synthesis of poly(aminomethyl acrylate) (PAMA)

6 mg TPO were added to a solution of 300 mg tBAMA in 300 μL 1,4-dioxane (50 wt%, M : I = 100 : 1). The mixture was placed in a UV cube for 5 minutes. 2.4 mL TFA were added and the mixture was stirred at 50 °C for 1 hour. The product was precipitated in methanol. Yield: 33%.

^{1}H-NMR. (300 MHz, $DMSO$): δ = 3.6 (3H, OCH$_3$), 2.1 (2H, CH$_2$).

^{13}C-NMR. (300 MHz, $DMSO$): δ = 181 (1C, COOMe), 60 (1C, OCH$_3$), 44 (1C, CH$_2$).

Synthesis of polydehydroalanine (PDha)

250 mg PAMA were dissolved in 10 mL 1,4-dioxane and a solution of 2.5 g LiOH ($\sim$45 eq.) in 10 mL H$_2$O was added. The mixture was stirred at 100 °C for 3 hours and neutralized with diluted HCl$_{aq.}$. During the neutralization, PDha precipitated. Yield: 97%.

^{1}H-NMR. (300 MHz, $D_2O/NaOD$, pH = 8): δ = 2,6 (b, 2H, CH$_2$).

Nanoparticle coating

SPION@PtBAA. 40 mg PtBAA were dissolved in 40 mL MilliQ water at pH = 12. To this solution, 40 mL of a dispersion of
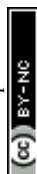
SPIONs (1 g L^{-1}) was added. The mixture was stirred at $50\,°C$ for 1 hour. The dispersion was centrifuged with 8000 rpm for 30 minutes, the supernatant was removed and the particles were redispersed in MilliQ water using ultrasonication. This procedure was repeated 5 times.

SPION@PAMA. 40 mg PAMA were dissolved in 40 mL DMSO. To this solution, 40 mL of a dispersion of SPIONs (1 g L^{-1}) was added. The mixture was stirred at $50\,°C$ for 1 hour. The dispersion was centrifuged with 8000 rpm for 30 minutes, the supernatant was removed and the particles were redispersed in DMSO using ultrasonication. This procedure was repeated 5 times.

SPION@PDha. 40 mg PDha were dissolved in 40 mL pH = 8 tris buffer. To this solution, 40 mL of a dispersion of SPIONs (1 g L^{-1}) was added. The mixture was stirred at $50\,°C$ for 1 hour. The dispersion was centrifuged with 8000 rpm for 30 minutes, the supernatant was removed and the particles were redispersed in pH = 8 tris buffer using ultrasonication. This procedure was repeated 5 times.

Size exclusion chromatography (SEC)

CHCl$_3$. SEC measurements were performed on a Shimadzu system equipped with a SCL-10A system controller, a LC-10AD pump, and a RID-10A refractive index detector using a solvent mixture containing chloroform, triethylamine, and isopropanol (94 : 4 : 2) at a flow rate of 1 mL min^{-1} on a PSS-SDV-linear M 5 μm column at $40\,°C$. The system was calibrated with PMMA (410–88 000 Da) standards.

DMAc. SEC measurements in dimethylacetamide (DMAc) were performed on an Agilent system equipped with G1310A pump, a G1362A refractive index detector, and both a PSS Gram30 and a PSS Gram1000 column in series. N,N-Dimethylacetamide with 2.1 g L^{-1} of LiCl was applied as eluent at 1 mL min^{-1} flow rate and the column oven was set to $40\,°C$.

DMSO. SEC measurements in DMSO were performed on a Jasco System equipped with a PU-980 pump, a DG-2080-53 degasser and a RI-930 refractive index detector. DMSO with 0.5% LiBr was used as solvent at a flow rate of 0.5 mL min^{-1} at $65\,°C$ on a PSS NOVEMA 3000/300 Å column. The system was calibrated with Pullulan standards.

H$_2$O. SEC measurements in water were performed on a Jasco System equipped with a PU-980 pump, a DG-2080-53 degasser and a RI-2031 Plus refractive index detector. Water with 0.01 M Na$_3$PO$_4$ was used as solvent at a flow rate of 1 mL min^{-1} at $30\,°C$ on a PSS SUPREMA pre/1000/100 Å column. The system was calibrated with PEO standards.

Zeta-potential measurements

The zeta-potentials were measured on a ZetaSizer Nano ZS from Malvern *via* M3-PALS technique with a laser beam at 633 nm. The detection angle was $13°$. The electrophoretic mobilities (u) were converted into zeta-potentials *via* the Henry equation in the Smoluchowski approximation, $\zeta = u_\eta / \varepsilon_0 \varepsilon$, where η denotes the viscosity and $\varepsilon_0 \varepsilon$ the permittivity of the solution.

Dynamic light scattering

Dynamic light scattering (DLS) measurements were performed using an ALV Laser CGS3 Goniometer equipped with a 633 nm HeNe Laser. DLS measurements were performed at $25\,°C$ and at a detection angle of $90°$. The CONTIN analysis of the obtained correlation functions was performed with the ALV 7002 FAST Correlator Software.

Static light scattering

Static light scattering (SLS) measurements were performed using an ALV Laser CGS3 Goniometer equipped with a 633 nm HeNe Laser. PtBAMA$_{184}$ was dissolved in methanol at five different concentrations (2, 3, 4, 5, 6 g L^{-1}). The dn/dc (0.152 mL g^{-1}) was measured on a Wyatt Technology Optilab-rEX Refractive Index Detector. SLS measurements were performed at $25\,°C$ and at detection angles from $20°$ to $150°$ in $5°$ steps. The measured data was evaluated using a ZIMM plot.

Vibrating sample magnetometry

VSM measurements were performed with a Micromag 3900, Princeton Measurement Corporation, at room temperature.

Transmission electron microscopy (TEM)

For TEM from aqueous dispersions, copper grids were rendered hydrophilic by Ar plasma cleaning for 30 s (Diener Electronics). 15 μL of the respective sample dispersion were applied to the grid and excess sample was blotted with a filter paper. TEM images were acquired with a 200 kV FEI Tecnai G^2 20 equipped with a 4k × 4k Eagle HS CCD and a 1k × 1k Olympus MegaView camera for overview images.

UV-irradiation

UV-irradiations were carried out using a Hoehnle UVACUBE 100 equipped with a 250 W lamp.

Ultrasonication

Ultrasonication was performed using an ElmaSonic S30H ultrasonic unit.

TGA

TGA measurements were carried out from room temperature up to $800\,°C$ under nitrogen with a Netzsch STA-449F1 device.

In vitro viability assay

Cytotoxic effects were investigated using a cell culture-based viability assay as described previously.[32] In brief, human brain microvascular endothelial cells (HBMEC) were cultured in RPMI 1640 supplemented with 10% fetal calf serum (FCS) at 37 $°C$ and 5% CO$_2$ in a humidified atmosphere. 45 000 cells per cm^2 were seeded into black-walled 96-well plates in quadruples and cultured overnight. Polyelectrolytes were added in concentrations as indicated; then, cell cultures were incubated for additional 3 h or 24 h, respectively. Polymer-associated effects on incubated cells were measured with the PrestoBlue

Cell Viability Assay (Invitrogen, Darmstadt, Germany). There, in presence of viable metabolically active cells the virtually non-fluorescent resazurin is reduced to highly fluorescent resufurin. Fluorescence signals were detected and quantified using the plate-reader Infinite M200 PRO (TECAN, Crailsheim, Germany).

Acknowledgements

References

1 P. Tartaj, M. d. P. Morales, S. Veintemillas-Verdaguer, T. González-Carreño and C. J. Serna, *J. Phys. D: Appl. Phys.*, 2003, **36**, R182–R197.
2 I. Coroiu, *J. Magn. Magn. Mater.*, 1999, **201**, 449–452.
3 W. H. Chiang, V. T. Ho, H. H. Chen, W. C. Huang, Y. F. Huang, S. C. Lin, C. S. Chern and H. C. Chiu, *Langmuir*, 2013, **29**, 6434–6443.
4 W. C. Dewey, *Int. J. Hyperthermia*, 1994, **10**, 457–483.
5 P. Wust, B. Hildebrandt, G. Sreenivasa, B. Rau, J. Gellermann, H. Riess, R. Felix and P. M. Schlag, *Lancet Oncol.*, 2002, **3**, 487–497.
6 R. K. Gilchrist, R. Medal, W. D. Shorey, R. C. Hanselman, J. C. Parrott and C. B. Taylor, *Ann. Surg.*, 1957, **146**, 506–606.
7 S. Dutz and R. Hergt, *Nanotechnology*, 2014, **25**, 452001.
8 M. W. Freeman, A. Arrott and J. H. L. Watson, *J. Appl. Phys.*, 1960, **31**, 404–406.
9 D. Schmaljohann, *Adv. Drug Delivery Rev.*, 2006, **58**, 1655–1670.
10 B. Mu, P. Liu, Y. Dong, C. Lu and X. Wu, *J. Polym. Sci., Part A: Polym. Chem.*, 2010, **48**, 3135–3144.
11 B. Mu, P. Liu, P. Du, Y. Dong and C. Lu, *J. Polym. Sci., Part A: Polym. Chem.*, 2011, **49**, 1969–1976.
12 J. Gao, H. Gu and B. Xu, *Acc. Chem. Res.*, 2009, **42**, 1097–1107.
13 K. Wormuth, *J. Colloid Interface Sci.*, 2001, **241**, 366–377.
14 X. Batlle and A. Labarta, *J. Phys. D: Appl. Phys.*, 2002, **35**, R15–R42.
15 J. Frenkel and J. Doefman, *Nature*, 1930, **126**, 274–275.
16 S. Tenzer, D. Docter, S. Rosfa, A. Wlodarski, J. Kuharev, A. Rekik, S. K. Knauer, C. Bantz, T. Nawroth, C. Bier, J. Sirirattanapan, W. Mann, L. Treuel, R. Zellner, M. Maskos, H. Schild and R. H. Stauber, *ACS Nano*, 2011, **5**, 7155–7167.
17 M. Lundqvist, J. Stigler, G. Elia, I. Lynch, T. Cedervall and K. A. Dawson, *Proc. Natl. Acad. Sci. U. S. A.*, 2008, **105**, 14265–14270.
18 C. D. Walkey, J. B. Olsen, H. Guo, A. Emili and W. C. Chan, *J. Am. Chem. Soc.*, 2012, **134**, 2139–2147.
19 M. Mahmoudi, A. M. Abdelmonem, S. Behzadi, J. H. Clement, S. Dutz, M. R. Ejtehadi, R. Hartmann, K. Kantner, U. Linne, P. Maffre, S. Metzler, M. K. Moghadam, C. Pfeiffer, M. Rezaei, P. Ruiz-Lozano, V. Serpooshan, M. A. Shokrgozar, G. U. Nienhaus and W. J. Parak, *ACS Nano*, 2013, **7**, 6555–6562.
20 D. Hühn, K. Kantner, C. Geidel, S. Brandholt, I. De Cock, S. J. H. Soenen, P. Rivera_Gil, J.-M. Montenegro, K. Braeckmans, K. Müllen, G. U. Nienhaus, M. Klapper and W. J. Parak, *ACS Nano*, 2013, **7**, 3253–3263.
21 G. Decher, *Science*, 1997, **277**, 1232–1237.
22 X. Hong, J. Li, M. Wang, J. Xu, W. Guo, J. Li, Y. Bai and T. Li, *Chem. Mater.*, 2004, **16**, 4022–4027.
23 B. Sun, Y. Zhang, K. J. Gu, Q. D. Shen, Y. Yang and H. Song, *Langmuir*, 2009, **25**, 5969–5973.
24 D. Yang, J. Ma, Q. Zhang, N. Li, J. Yang, P. A. Raju, M. Peng, Y. Luo, W. Hui, C. Chen and Y. Cui, *Anal. Chem.*, 2013, **85**, 6688–6695.
25 B. Mu, W. Zhong, Y. Dong, P. Du and P. Liu, *J. Biomed. Mater. Res., Part B*, 2012, **100**, 825–831.
26 J. Wotschadlo, T. Liebert, J. H. Clement, N. Anspach, S. Hoppener, T. Rudolph, R. Müller, F. H. Schacher, U. S. Schubert and T. Heinze, *Macromol. Biosci.*, 2013, **13**, 93–105.
27 J. Wotschadlo, T. Liebert, T. Heinze, K. Wagner, M. Schnabelrauch, S. Dutz, R. Müller, F. Steiniger, M. Schwalbe, T. C. Kroll, K. Höffken, N. Buske and J. H. Clement, *J. Magn. Magn. Mater.*, 2009, **321**, 1469–1473.
28 L. C. Fidale, M. Nikolajski, T. Rudolph, S. Dutz, F. H. Schacher and T. Heinze, *J. Colloid Interface Sci.*, 2013, **390**, 25–33.
29 A. Kaiser, S. Dutz and A. M. Schmidt, *J. Polym. Sci., Part A: Polym. Chem.*, 2009, **47**, 7012–7020.
30 U. Günther, L. V. Sigolaeva, D. V. Pergushov and F. H. Schacher, *Macromol. Chem. Phys.*, 2013, 2202–2212.
31 S. Dutz, W. Andrä, R. Hergt, R. Müller, C. Oestreich, C. Schmidt, J. Töpfer, M. Zeisberger and M. E. Bellemann, *J. Magn. Magn. Mater.*, 2007, **311**, 51–54.
32 F. Bähring, F. Schlenk, J. Wotschadlo, N. Buske, T. Liebert, C. Bergemann, T. Heinze, A. Hochhaus, D. Fischer and J. H. Clement, *IEEE Trans. Magn.*, 2013, **49**, 383–388.